Interplay of the magnetic and current density field topologies in axisymmetric devices for magnetic confinement fusion

Marie-Christine Firpo

Interplay of the magnetic and current density field topologies in axisymmetric devices for magnetic confinement fusion

Marie-Christine A. Firpo
Laboratoire de Physique des Plasmas (LPP), CNRS, Sorbonne Université, Ecole polytechnique, Institut Polytechnique de Paris, 91120 Palaiseau, France

Under review - May, 31 2024

Abstract
In magnetic confinement fusion devices close to axisymmetry, such as tokamaks, a key element is the winding profile of the magnetic field lines, or its inverse, the safety profile $q = q_{\mathbf{B}}$. A corresponding profile, $q_{\mathbf{J}}$, can be defined for the current density field lines. Ampère's law relates any mode of current perturbation $\delta\mathbf{J}_{m,n}$ with a mode of magnetic perturbation $\delta\mathbf{B}_{m,n}$. It is shown that the knowledge of the pair $(q_{\mathbf{B}}, q_{\mathbf{J}})$ allows then to characterize the resonant, or non-resonant, nature of the modes for both the magnetic and current density field lines. The expression of $q_{\mathbf{J}}$ in flux coordinate is derived. Including this calculation in the real-time Grad-Shafranov equilibrium reconstruction codes would yield a comprehensive view of the magnetics. The monitoring of the pair $(q_{\mathbf{B}}, q_{\mathbf{J}})$ would then allow investigating the role played by the resonant modes for the current density, that are current filamentary modes, in the plasma small-scale turbulence. By driving the magnetic and current density profiles apart so that the images of $q_{\mathbf{B}}$ and $q_{\mathbf{J}}$ are disjoint, these filamentary modes would not impact the magnetic field topology, being not associated to magnetic islands but to non-resonant magnetic modes. It remains to be explored to which extent such a configuration, where the spectrum of tiny current density filaments produces a spectrum of magnetic modes that has practically no effect on heat transport, is beneficial.

1 Introduction

In a magnetic confinement fusion (MCF) plasma, alpha particles produced from fusion reactions will be confined by the magnetic field and heat back the plasma species, and primarily electrons, through collisions. To ignite the plasma, the rate of alpha heating must exceed (and at least match) the rate at which plasma loses energy. Finding scenarios that minimize plasma losses is thus crucial for optimizing the achievement of the conditions necessary for fusion and sustained ignition. A well-known prime reservoir for the minimization of plasma losses lies in the electron energy channel since the electron heat transport is anomalous. This arises from the fact that being the least massive charged particles, electrons are also the most magnetized and thus the most sensitive to the non-regularity of magnetic field lines. Understanding, controlling and ideally reducing electron heat transport has thus been a major objective of MCF research so far.

A picture that emerged long ago is that the magnetic topology impacts then the electron collective behaviour. Ideally, the magnetic field within a tokamak should be axisymmetric with smooth magnetic field lines spiralling about the magnetic axis. Yet, departures from axisymmetry caused by 3D effects manifesting through the overlap of magnetic resonances break the smoothness of the magnetic field lines and introduce, at least locally, some stochasticity. Although a rigorously exact self-consistent analysis of electron heat transport may still be mathematically out-of-reach, some relevant estimates obtained using simplifying assumptions exist for long. A significant breakthrough occurred when Rechester and Rosenbluth [1] showed that, because electrons are strongly magnetized, even a slight braiding of magnetic field lines could result in a noticeable increase in perpendicular heat transport. This means that the magnetic field lines diffusivity transfers to the electron thermal diffusivity. This derivation was done under the assumption of stationary magnetic fluctuations and prompted numerous theoretical studies aiming to clarify its application regime. Later, Isichenko notably included the decorrelation effects produced by time-varying magnetic perturbations [2, 3]. It emerges from this careful analysis that, except for the extreme case of quick decorrelation where the characteristic frequency of magnetic turbulence would be much greater than the ratio of the electron thermal velocity, v_e, to the magnetic exponentiation length, the electron thermal diffusivity is proportional to the magnetic line diffusivity D_m. Furthermore, in the collisionless limit, it approximates to $v_e D_m$.

Critical to the anomalous electron transport is thus the existence of *resonant* magnetic perturbations. This calls for an examination of the source of these resonant magnetic perturbations. In addition to some possible curl-free magnetic perturbations coming from external sources, e.g. due to ripple effects, the magnetic perturbations are associated by Ampère's law to plasma current density perturbations. This naturally introduces a plasma current density approach that has been left apart up to now. Indeed, in a tokamak plasma, the displacement current is largely negligible in front of the plasma current so that the

plasma current density, $\mathbf{J}$, can be approximated as a divergence-free field satisfying

$$\mathbf{J} = \mu_0^{-1} \nabla \times \mathbf{B}. \tag{1}$$

Equation (1), together with the Maxwell-flux equation

$$\nabla \cdot \mathbf{B} = 0, \tag{2}$$

form then a closed set of equations. It is the aim of the present Letter to explore the implications of the divergence-free nature of the magnetic and current density fields linked by Ampère's law (1) in driven MCF ideally-axisymmetric devices such as tokamaks.

2 Hamiltonian representation of divergence-free field fieldlines

At each given time, Eq. (2) is universally valid and Eq. (1) is a strongly relevant approximation in tokamak plasmas since the magnitude of the displacement current density $\mathbf{J}_d = c^{-2}\partial_t \mathbf{E}$ is at least eleven orders smaller than that of the plasma current density [4]. Yet, the field lines of any solenoidal (i.e. divergence-free) field can be identified to the trajectories of a one-and-a-half degrees of freedom Hamiltonian system. Here, this means that, at each *given* time t, magnetic and current density field lines are the respective trajectories of two Hamiltonian systems $H^t_{\mathbf{B}}$ and $H^t_{\mathbf{J}}$ depending on three space coordinates. In a simple toroid, the divergence-free vector fields $\mathbf{B}$ and $\mathbf{J}$ may be represented in the general canonical forms [5–7]

$$\mathbf{B} = \nabla\psi_{\mathbf{B}} \times \nabla\theta + \nabla\varphi \times \nabla H^t_{\mathbf{B}}, \tag{3}$$

$$\mathbf{J} = \nabla\psi_{\mathbf{J}} \times \nabla\theta + \nabla\varphi \times \nabla H^t_{\mathbf{J}}, \tag{4}$$

where θ and φ are independent appropriate poloidal and toroidal angles. The differential equations to solve to obtain the magnetic field lines are

$$\frac{d\psi_{\mathbf{B}}}{d\varphi} = \frac{\mathbf{B}\cdot\nabla\psi_{\mathbf{B}}}{\mathbf{B}\cdot\nabla\varphi} = -\frac{\partial H^t_{\mathbf{B}}}{\partial\theta},$$

$$\frac{d\theta}{d\varphi} = \frac{\mathbf{B}\cdot\nabla\theta}{\mathbf{B}\cdot\nabla\varphi} = \frac{\partial H^t_{\mathbf{B}}}{\partial\psi_{\mathbf{B}}},$$

with similar equations for $\mathbf{J}$-field lines. Generically, the Hamiltonian $H^t_{\mathbf{B}}(\psi_{\mathbf{B}}, \theta, \varphi)$ can be Fourier decomposed into an axisymmetric equilibrium part depending on the flux function $\psi_{\mathbf{B}}$ and a non-axisymmetric perturbation part such that

$$H^t_{\mathbf{B}}(\psi_{\mathbf{B}}, \theta, \varphi) = H^t_{\mathbf{B}0}(\psi_{\mathbf{B}}) + \sum_{(m,n)\neq(0,0)} h^t_{\mathbf{B}mn}(\psi_{\mathbf{B}}) \cos\left(m\theta - n\varphi + \chi^t_{\mathbf{B}mn}\right). \tag{5}$$

For simplicity's sake, the time t index will be dropped in the following. The axisymmetric contribution is dominant in tokamak plasmas and yields integrable magnetic and density field lines spiraling on flux surfaces given by

$$\psi_{\mathbf{B}} = const, \frac{d\theta}{d\varphi} = \frac{dH_{\mathbf{B}0}}{d\psi_{\mathbf{B}}} \equiv q^{-1}_{\mathbf{B}}(\psi_{\mathbf{B}}),$$

$$\psi_{\mathbf{J}} = const, \frac{d\theta}{d\varphi} = \frac{dH_{\mathbf{J}0}}{d\psi_{\mathbf{J}}} \equiv q^{-1}_{\mathbf{J}}(\psi_{\mathbf{J}}).$$

defining the magnetic and current density "safety factor" functions $q_{\mathbf{B}} = q$ and $q_{\mathbf{J}}$. Let us note here that, under the usual assumption that the Grad-Shafranov equation holds at equilibrium, both magnetic and current density flux surfaces are constant pressure surfaces which allows to construct a common set of canonical coordinates to express $\mathbf{B}$ and $\mathbf{J}$, such as Hamada coordinates [8, 9]. For the present analysis, it is sufficient that the same poloidal and toroidal coordinates be shared by $\mathbf{B}$ and $\mathbf{J}$ canonical descriptions. Let us note also that, in fusion-relevant tokamaks, diamagnetic effects ensure that $q_{\mathbf{J}}$ is not trivial.

3 Topology and classification of modes

Let us consider a perturbation to the axisymmetric state by a single mode (m_0, n_0). The generic form of the Hamiltonian, for the $\mathbf{B}$- or $\mathbf{J}$-field lines, is then

$$H(\psi, \theta, \varphi) = H_0(\psi) + \varepsilon h(\psi) \cos(m_0\theta - n_0\varphi + \chi_0). \tag{6}$$

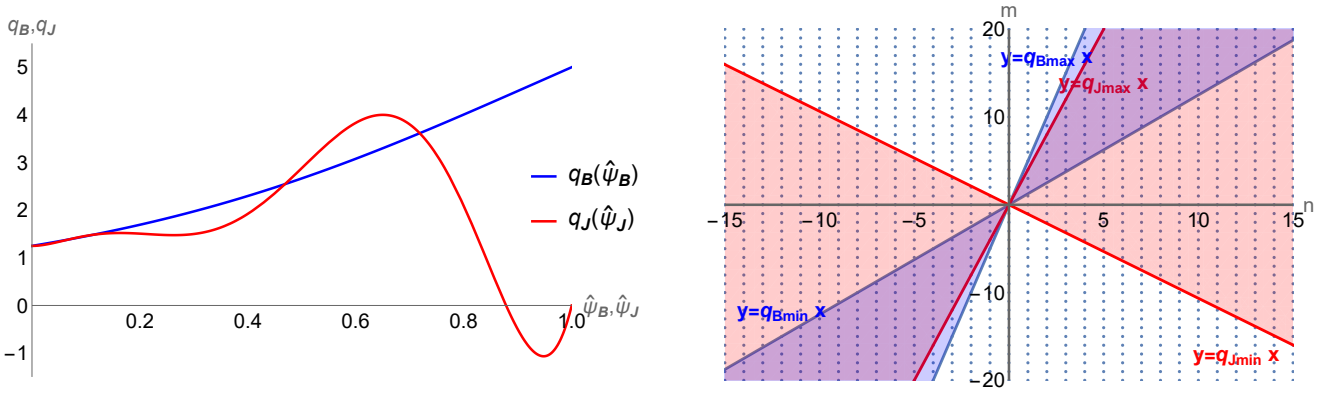

Figure 1: Left) Example of two arbitrary magnetic and current density safety factor profiles as a function of resp. normalized flux coordinates $\widehat{\psi}_{\mathbf{B}}$ and $\widehat{\psi}_{\mathbf{J}}$. Right) Each dot represents an (m, n) mode. It is a resonant mode for $\mathbf{B}$ if it is in the blue cone bounded by the lines $y = q_{\mathbf{B}\,\min} x$ and $y = q_{\mathbf{B}\,\max} x$ and/or for $\mathbf{J}$ if it is in the red cone bounded by the lines $y = q_{\mathbf{J}\,\min} x$ and $y = q_{\mathbf{J}\,\max} x$. The violet intersection cone contains modes that are both resonant to $\mathbf{B}$ and $\mathbf{J}$. The white cone contains modes that are non-resonant to $\mathbf{B}$ and non-resonant to $\mathbf{J}$.

Resonance occurs when the insertion of the $O(\varepsilon^0)$ axisymmetric solution produces a secular forcing resulting in a linear increase of ψ with φ. This happens when there exists some ψ^* such that $q(\psi^*) = m_0/n_0$. Figure 1 considers an instantaneous axisymmetric plasma state with *arbitrary* magnetic and current density safety profiles. The plot on the right highlights the possible resonant modes for $\mathbf{B}$ (in blue) and for $\mathbf{J}$ (in red). On this example, there are modes that are both resonant for $\mathbf{B}$ and $\mathbf{J}$ in the overlapping (violet) cone. By virtue of the linearity of Ampère's equation (1), some (m_0, n_0) current perturbation $\delta\mathbf{J}_{m_0,n_0}$ is associated to some (m_0, n_0) magnetic perturbation $\delta\mathbf{B}_{m_0,n_0}$. Reciprocally, there could exist vacuum magnetic perturbations that have no manifestation on the current density. Since our interest lies in the magnetic perturbations originating from plasma current density perturbations, we focus on the current density modes.

Any mode of a divergence-free vector field with a rotational transform is either resonant or non-resonant. Considering the current density field $\mathbf{J}$, a mode (m_0, n_0) is resonant if there exists some $\psi^*_{\mathbf{J}}$ such that $q(\psi^*_{\mathbf{J}}) = m_0/n_0$; if not, it is non-resonant. In the first case, a poloidal cross-section cut of the current density field lines reveals that, around the current flux surface $\psi^*_{\mathbf{J}}$, even a tiny amplitude (m_0, n_0) perturbation produces a change in the topology of current density field lines with the apparition of a vortex (island). In 3D, such a resonant mode for the current density exhibits then a filamentary structure such as in the example of Figure 2. On the contrary, a non-resonant mode manifests only through smooth deformations of flux contours. To be more specific, a resonant mode (m_0, n_0) for $\mathbf{B}$ originating from a current density perturbation can have for source either a $\mathbf{J}$-resonant filament-like mode if there exists some $\psi^*_{\mathbf{J}}$ such that $q(\psi^*_{\mathbf{J}}) = m_0/n_0$ (this is the case for modes in the violet cone of Fig. 1), either a non-resonant $\mathbf{J}$ mode if not (this is the case for modes in the blue region of Fig. 1). Non-resonant modes include collective modes of deformation of the current density radial contours.

4 Illustration in cylindrical geometry of the interplay between magnetic and current density field topologies

Let us examine this further by deriving the magnetic and current density field lines corresponding to some axisymmetric state, defined by given $q_{\mathbf{B}}$ and $q_{\mathbf{J}}$, perturbed by a single mode with poloidal mode number m_0 and toroidal mode number n_0. Here we shall consider a cylinder configuration with length $2\pi R$ with periodic boundary conditions ($z = R\varphi$) to simplify calculations without affecting the conclusions. One simplification of cylindrical geometry is that the action variable ψ only depends on the radius r so that we can directly use r to compare $q_{\mathbf{B}}$ and $q_{\mathbf{J}}$.

The axisymmetric axial component of the magnetic field is denoted by $B_0(r)$ and $B_0(0) \equiv B_0$. The total magnetic field amounts to $\mathbf{B} = B_\theta(r)\mathbf{e}_\theta + B_0(r)\mathbf{e}_z + \delta\mathbf{B}(r, \theta, z)$ with $\delta\mathbf{B}(r, \theta, z) = \nabla \times \delta\mathbf{A}$ with $\delta\mathbf{A} = \varepsilon_{m_0,n_0} f(r) \cos(m_0\theta - n_0\varphi)\mathbf{e}_z$, for some waveform $f(r)$. The total current density field is obtained from Ampère's law (1). The equations of the magnetic field lines derive from $\mathbf{B} \times d\mathbf{OM} = \mathbf{0}$ with $d\mathbf{OM} = dr\mathbf{e}_r + rd\theta\mathbf{e}_\theta + dz\mathbf{e}_z$ and similarly for the current density field lines. For the equilibrium

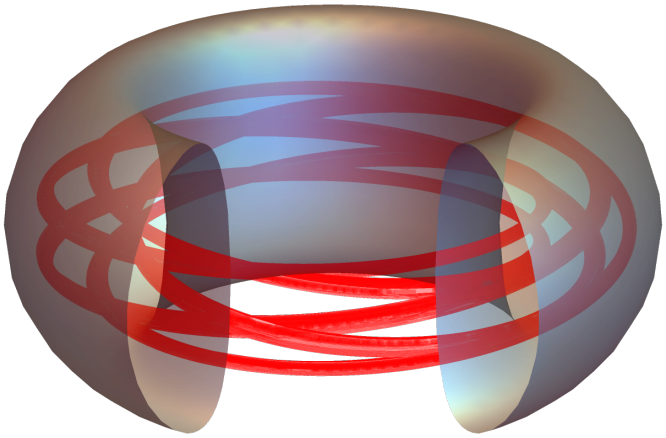

Figure 2: When there exists some $\psi^*_{\mathbf{J}}$ such that $q(\psi^*_{\mathbf{J}}) = m_0/n_0$, i.e. the mode (m_0, n_0) is resonant for $\mathbf{J}$, then a current filament flows within the current "flux tubes" attached to elliptic surfaces. In the representation, $m_0 = 5$ and $n_0 = 3$.

axisymmetric part, one obtains the expressions of $q_{\mathbf{B}}$ and $q_{\mathbf{J}}$ as functions of the magnetic field components

$$q_{\mathbf{B}}(r) = \frac{rB_0(r)}{RB_\theta(r)}, \tag{7}$$

$$q_{\mathbf{J}}(r) = -\frac{B_\theta(r) + rB'_\theta(r)}{RB_0(r)}. \tag{8}$$

Considering given radial profiles $q_{\mathbf{B}}(r)$ and $q_{\mathbf{J}}(r)$, the system (7)-(8) allows to obtain the axisymmetric magnetic field components as $B_\theta(r) = rB_0(r)/(Rq_{\mathbf{B}}(r))$ with the axial component $B_0(r)$ solving a first order differential equation as

$$B_0(r) = B_0 \exp\left(\int_0^r \frac{x^2 q'_{\mathbf{B}}(x) - 2xq_{\mathbf{B}}(x)}{R^2 q^2_{\mathbf{B}}(x) q_{\mathbf{J}}(x) + x^2 q_{\mathbf{B}}(x)} dx\right). \tag{9}$$

The winding properties of the axisymmetric equilibrium magnetic and current density fields are specified by the pair $(q_{\mathbf{B}}, q_{\mathbf{J}})$. In Figure 3, a safety profile $q_{\mathbf{B}}$ has been chosen. We consider the effect of a small perturbation having $m_0 = 5$ and $n_0 = 3$ that is resonant for the magnetic field because there exists some minor radius at which $q_{\mathbf{B}} = 5/3$. This determines the Poincaré plot of magnetic field lines, shown in blue on Figure 3c). The Poincaré plots of the current density field lines are plotted in red and vary according to the $q_{\mathbf{J}}$ profile. For each $q_{\mathbf{J}}$, the components of the magnetic field (normalized to B_0) are fully known and are plotted for the sake of completeness in Fig. 3b). Depending on $q_{\mathbf{J}}$, the magnetic island is associated either to a current density island (or filamentation mode), if there exists one radial coordinate at which $q_{\mathbf{J}} = m_0/n_0$ (case $q_{\mathbf{J}1}$) or more than one (case $q_{\mathbf{J}2}$). Let us note that the radial locations of the magnetic and current density islands differ when $q_{\mathbf{B}}$ and $q_{\mathbf{J}}$ do not coincide, which is the case considered here. Alternatively, the magnetic island may be associated to a non-resonant current density mode when $q_{\mathbf{J}}$ does not take the value m_0/n_0 (cases 3 and 5). The case 4 corresponds to a limiting case when $q_{\mathbf{J}}$ reaches the value m_0/n_0 at the border.

It has been shown that providing the pair $(q_{\mathbf{B}}, q_{\mathbf{J}})$ allows for a comprehensive characterization of the modes. This requires to reconstruct in real time not only the safety profile, $q_{\mathbf{B}}$, but also $q_{\mathbf{J}}$. To facilitate this in the realistic toroidal geometry, their expression in flux coordinates are derived now.

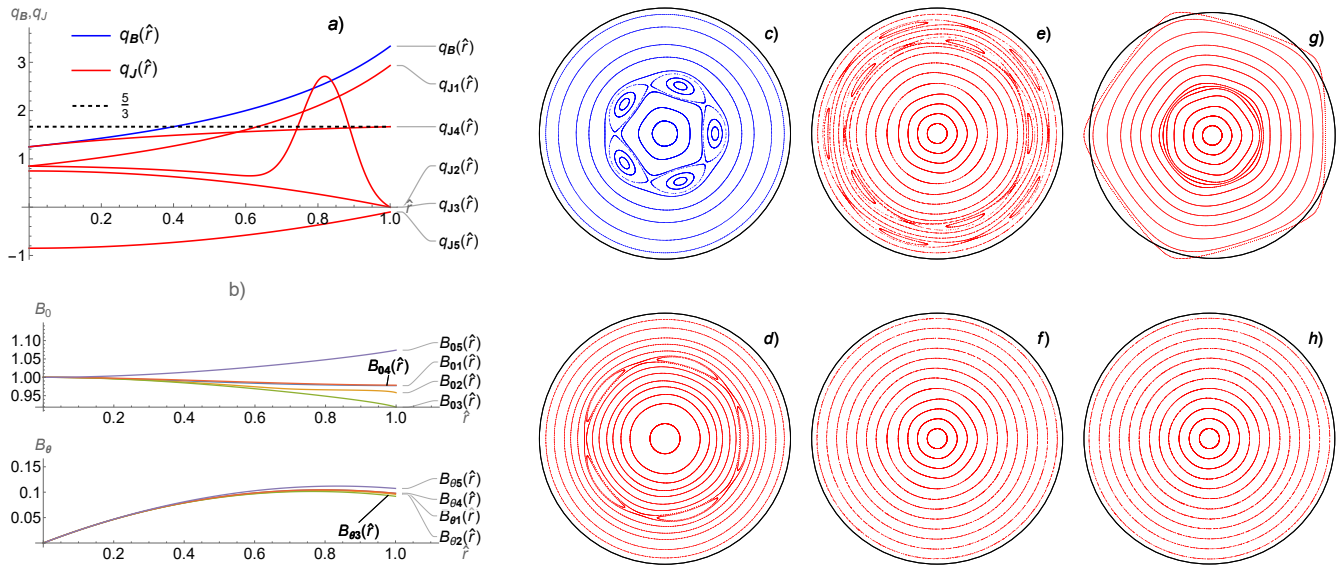

Figure 3: Examples of the impact on magnetic and current density field lines of a small 3D perturbation, having here poloidal $m_0 = 5$ and toroidal $n_0 = 3$ mode numbers. The arbitrarily chosen safety profile $q_{\mathbf{B}}$ is plotted in blue in a). The Poincaré's plot of the magnetic field lines is shown in c) and shows that the perturbation is magnetically-resonant. One considers five arbitrary $q_{\mathbf{J}}$-profiles, noted $q_{\mathbf{J}1}$ to $q_{\mathbf{J}5}$, plotted in red in a). The corresponding current density field lines are plotted in d), e), f), g) and h). Knowing $q_{\mathbf{B}}$ and $q_{\mathbf{J}}$ provides the full axisymmetric magnetic configuration b) (normalized to B_0). $\hat{r}$ denotes the radial variable normalized to the minor radius.

5 Analytic expressions of the magnetic ($q_{\mathbf{B}}$) and current density ($q_{\mathbf{J}}$) profiles in flux coordinates

In the Hamada set of variables (v, θ, ζ), with v the volume enclosed by the flux surface, and ζ and θ the toroidal and poloidal coordinates (chosen here to have period 1, not 2π), both equilibrium magnetic and current density field lines are straigth with

$$\begin{aligned} q_{\mathbf{B}}(v) &= \frac{\mathbf{B}.\nabla\zeta}{\mathbf{B}.\nabla\theta}, \\ q_{\mathbf{J}}(v) &= \frac{\mathbf{J}.\nabla\zeta}{\mathbf{J}.\nabla\theta}. \end{aligned}$$

This is a canonical set of variables for both the magnetic and current density field lines. It is however not easy to accomodate because the toroidal and poloidal coordinates are not the usual geometrical angles. Nevertheless, the previous illustration (in Fig. 3) as well as the diagramm (in Fig. 1) show that, in order to classify modes, we essentially need to compare the equilibrium windings of the magnetic field and the current density field. Using the explicit transformation between Hamada coordinates (v, θ, ζ) and the flux coordinates $\left(\psi, \theta_g, \varphi_g\right)$, where θ_g and φ_g are respectively the poloidal and toroidal geometrical angles, it was shown in [10] that $q_{\mathbf{B}}(v)$ is the usual safety factor, namely

$$q_{\mathbf{B}}(v) = \frac{1}{2\pi} \oint_{\psi} \frac{\mathbf{B}.\nabla\varphi_g}{\mathbf{B}.\nabla\theta_g} d\theta_g = q_{\mathbf{B}}(\psi). \tag{10}$$

Moreover, using $\mathbf{B} = F(\psi)\nabla\varphi_g + \nabla\psi\times\nabla\varphi_g$ [signe] where $F(\psi) = RB_{\varphi_g}$ is the diamagnetic function, and defining the flux surface average

$$\langle X \rangle \doteq \left(\oint_{\psi} \frac{d\theta'_g}{\mathbf{B}.\nabla\theta'_g} \right)^{-1} \oint_{\psi} \frac{X d\theta'_g}{\mathbf{B}.\nabla\theta'_g} = \frac{\partial}{\partial v} \int_V X dv', \tag{11}$$

yields

$$q_{\mathbf{B}}(v) = \frac{F(\psi)}{2\pi} \oint R^{-2} \frac{d\theta_g}{\mathbf{B}.\nabla\theta_g} = \frac{F(\psi)}{4\pi^2} \left\langle R^{-2} \right\rangle v'(\psi). \tag{12}$$

Now let us also consider here $q_{\mathbf{J}}$. We have

$$\begin{aligned}\mathbf{J}.\nabla\zeta &= \frac{1}{2\pi}\mathbf{J}.\nabla\varphi_g + \frac{F(\psi)}{2\pi}\left(\left\langle R^{-2}\right\rangle - R^{-2}\right)\frac{\mathbf{J}.\nabla\theta_g}{\mathbf{B}.\nabla\theta_g},\\ \mathbf{J}.\nabla\theta &= \frac{\mathbf{B}.\nabla\theta}{\mathbf{B}.\nabla\theta_g}\mathbf{J}.\nabla\theta_g.\end{aligned}$$

Moreover,

$$\theta\left(\psi,\theta_g\right) = \left(\oint\frac{d\theta'_g}{\mathbf{B}.\nabla\theta'_g}\right)^{-1}\int_0^{\theta_g}\frac{d\theta'_g}{\mathbf{B}.\nabla\theta'_g}, \tag{13}$$

implying

$$\frac{\partial\theta_g}{\partial\theta} = \left(\oint\frac{d\theta'_g}{\mathbf{B}.\nabla\theta'_g}\right)\mathbf{B}.\nabla\theta_g. \tag{14}$$

We have, from Eq. (13) and (13),

$$q_{\mathbf{J}}(v) = \frac{\mathbf{J}.\nabla\zeta}{\mathbf{J}.\nabla\theta} = \frac{1}{2\pi}\frac{\mathbf{J}.\nabla\varphi_g}{\mathbf{J}.\nabla\theta_g}\frac{\mathbf{B}.\nabla\theta_g}{\mathbf{B}.\nabla\theta} + \frac{F(\psi)}{2\pi}\frac{\left\langle R^{-2}\right\rangle - R^{-2}}{\mathbf{B}.\nabla\theta}. \tag{15}$$

Let us use the fact that we can average "for free" this function on θ as it only depends on v. We have, for the first member of the right hand side

$$\oint\frac{1}{2\pi}\frac{\mathbf{J}.\nabla\varphi_g}{\mathbf{J}.\nabla\theta_g}\frac{\mathbf{B}.\nabla\theta_g}{\mathbf{B}.\nabla\theta}d\theta = \oint\frac{1}{2\pi}\frac{\mathbf{J}.\nabla\varphi_g}{\mathbf{J}.\nabla\theta_g}d\theta_g. \tag{16}$$

For the second member of the right hand side, we have

$$\oint\frac{F(\psi)}{2\pi}\frac{\left\langle R^{-2}\right\rangle - R^{-2}}{\mathbf{B}.\nabla\theta}d\theta = \oint\frac{F(\psi)}{2\pi}\frac{\left\langle R^{-2}\right\rangle - R^{-2}}{\mathbf{B}.\nabla\theta_g}d\theta_g = 0 \tag{17}$$

by definition of the flux surface average (11). This gives the result

$$q_{\mathbf{J}}(v) = \frac{1}{2\pi}\oint\frac{\mathbf{J}.\nabla\varphi_g}{\mathbf{J}.\nabla\theta_g}d\theta_g. \tag{18}$$

Let us now use the Grad-Shafranov equation to get an explicit expression. This gives

$$\mathbf{J}.\nabla\varphi_g = \frac{dp}{d\psi} + \frac{1}{\mu_0 R^2}F\frac{dF}{d\psi}. \tag{19}$$

From $\mu_0\mathbf{J}.\nabla\theta_g = \left(\nabla F\times\nabla\varphi_g\right).\nabla\theta_g$, $\mathbf{B}.\nabla\theta_g = \left(\nabla\psi\times\nabla\varphi_g\right).\nabla\theta_g$ and $\nabla F = F'(\psi)\nabla\psi$, one gets $\mathbf{J}.\nabla\theta_g = \mu_0^{-1}F'(\psi)\mathbf{B}.\nabla\theta_g$. Consequently,

$$\begin{aligned}q_{\mathbf{J}}(v) &= \frac{1}{2\pi}\oint\frac{\mu_0 p'(\psi) + \frac{FF'(\psi)}{R^2}}{F'(\psi)\mathbf{B}.\nabla\theta_g}d\theta_g\\ &= \frac{1}{2\pi}\oint\frac{\mu_0 p'(\psi)}{F'(\psi)\mathbf{B}.\nabla\theta_g}d\theta_g + \frac{1}{2\pi}\oint\frac{F(\psi)}{R^2\mathbf{B}.\nabla\theta_g}d\theta_g\\ &= \frac{\mu_0 p'(\psi)}{F'(\psi)}\frac{1}{2\pi}\oint\frac{d\theta_g}{\mathbf{B}.\nabla\theta_g} + q_{\mathbf{B}}(v).\end{aligned}$$

This yields from (11) and (12)

$$q_{\mathbf{J}}(v) - q_{\mathbf{B}}(v) = \frac{\mu_0}{4\pi^2}\frac{p'(\psi)v'(\psi)}{F'(\psi)} \tag{20}$$

that is, choosing the flux label ψ instead of v,

$$q_{\mathbf{J}}(\psi) = q_{\mathbf{B}}(\psi)\left[1 + \frac{\mu_0 p'(\psi)}{\left\langle R^{-2}\right\rangle FF'(\psi)}\right]. \tag{21}$$

To the author's knowledge, this is the first expression of the $q_{\mathbf{J}}$ profile in flux coordinates. We are indeed in the same situation as in the previous cylindrical illustration where the action variable depends only on the radius r: Here, the action variable v in the Hamada's set depends only on ψ ($v = v(\psi)$). One can then do the comparison between the $q_{\mathbf{B}}$ and $q_{\mathbf{J}}$ profiles with flux coordinates. This can serve to figure out whether the modes resonant to the current density, namely the current filamentary modes, produce magnetic perturbations that are resonant to the magnetic field.

6 Implications, perspectives and conclusions

In the case of a zero-β (constant zero pressure) plasma, Eq. (21) shows that $q_{\mathbf{B}}$ and $q_{\mathbf{J}}$ coincide. In this special case, (m, n) current filaments flow within (m, n) magnetic islands. This case is not relevant to fusion conditions. Indeed, in ITER, to attain $Q \simeq 10$, plasmas will need to have a normalized beta $\beta_N > 1.8$ with $\beta_N = \beta/I/aB$, I the plasma current, a the minor radius and $\beta \equiv p/B^2/(2\mu_0)$ [11]. Consequently, the $q_{\mathbf{J}}$ profile will be somehow separated from the $q_{\mathbf{B}}$ profile according to Eq. (21). In view of the one-and-a-half Hamiltonian picture of the field lines, this means that a MCF device needs to *drive the magnetic and current density channels apart*. The present study should thus have important implications:

i. Add the calculation of $q_{\mathbf{J}}$ to equilibrium reconstruction codes to diagnose the separation of the magnetic and current density channels.

   The kinetic equilibrium reconstruction codes presently serve to monitor in real time the magnetics in modern tokamaks. This involves the resolution of the elliptic nonlinear Grad-Shafranov differential equation to determine the magnetic equilibrium configuration from the measurement data. This has been a challenging and fundamental MCF research topic for around four decades, involving the collaborative contributions of physicists, mathematicians and computer scientists [12–24], with recent contributions from fast-parallel computing [25], artificial intelligence and neural networks [26–30].

   One outcome of these codes is the real-time computation of the safety factor profile q (that is $q_{\mathbf{B}}$). The analysis presented here highlights the value of including the computation of the current density $q_{\mathbf{J}}$ profile. It is shown by Eq. (21) that this amounts to add just a line to existing codes. Then, the knowledge of the pair $(q_{\mathbf{B}}, q_{\mathbf{J}})$ will enable the complete identification of the electromagnetic, not purely electrostatic, modes, both in terms of their magnetic contribution and their contribution to the current density, as exemplified in Figure 1.

   Let us here note that the expression for $q_{\mathbf{J}}$ in Eq. (21) has been obtained under the usual assumption that the plasma equilibrium is governed by the Grad-Shafranov equation. This derives from the steady-state Navier-Stokes equation in which one neglects the plasma velocity field. If this steady-state plasma velocity field happens to be non negligible then plasma rotation could also contribute to separate the magnetic and current density channels. Nevertheless, one can reasonably expect the Grad-Shafranov equation to give the dominant contribution to $q_{\mathbf{J}}$.

ii. Investigate the relationship between the interplay of the $q_{\mathbf{B}}$ and $q_{\mathbf{J}}$ profiles and the confinement properties.

   Any experimentally-unavoidable perturbation to the axisymmetric current density gives rise, through Fourier mode decomposition, to a spectrum of current density modes. In particular, there exists, at any time, a spectrum of tiny filamentation modes, that are modes for which $q_{\mathbf{J}}$ is rational. Obviously, linear theory may favor some specific modes. The point here is just to stress that there should exist at all times a spectrum of non-vanishing current density filaments that comes up, by the virtue of Ampère's law, with a spectrum of magnetic perturbations.

   Let us consider, for example, a situation where the images of the functions $q_{\mathbf{B}}$ and $q_{\mathbf{J}}$ are *disjoint*. Then, the resonant modes for the current density (i.e. the filamentary modes) do not impact the magnetic field topology. They are not associated to magnetic islands, but to non-resonant magnetic modes. In this case, only collective modes of deformation of the current density, that do not change the topology of the current density field lines, can be associated to magnetic islands. It remains to be explored to which extent such a configuration, where the spectrum of tiny current density filaments produces a spectrum of magnetic modes that has practically no effect on heat transport, is beneficial.

iii. Explore the possibility of controlling the current transport and preventing disruptions by playing on the current density profile.

   In MCF devices such as tokamaks, apart from magnetic perturbations due to the vacuum configuration, such as the ripple-induced magnetic disturbances, one can consider the current density channel as the driver for magnetic perturbations. By separating the $q_{\mathbf{B}}$ and $q_{\mathbf{J}}$ profiles, one can prevent the magnetic perturbations due to the aforementioned tiny current filaments to contribute to magnetic diffusivity. Ultimately, the current path might also be controlled by monitoring and playing on the shear of the $q_{\mathbf{J}}$ profile with potentially important implications.

   In conclusion, this Letter points to the benefits of monitoring both the $q_{\mathbf{B}}$ and $q_{\mathbf{J}}$ profiles to get a full, real-time, picture of the magnetic and current density channels in MCF devices. Some reconstruction of the $q_{\mathbf{J}}$ profile from experimental data will be presented and analysed in a forthcoming study.

References

[1] A. B. Rechester and M. N. Rosenbluth. Electron heat transport in a tokamak with destroyed magnetic surfaces. Phys. Rev. Lett., 40:38–41, Jan 1978.

[2] M B Isichenko. Effective plasma heat conductivity in 'braided' magnetic field-i. quasi-linear limit. Plasma Physics and Controlled Fusion, 33(7):795, jul 1991.

[3] M B Isichenko. Effective plasma heat conductivity in 'braided' magnetic field-ii. percolation limit. Plasma Physics and Controlled Fusion, 33(7):809, jul 1991.

[4] Allen H. Boozer. Non-axisymmetric magnetic fields and toroidal plasma confinement. Nuclear Fusion, 55(2):025001, jan 2015.

[5] Allen H. Boozer. Evaluation of the structure of ergodic fields. The Physics of Fluids, 26(5):1288–1291, 05 1983.

[6] Tadatsugu Hatori, Haruyuki Irie, Yoshihiko Abe, and Kazuhiro Urata. Chaotic mgnetic field line in toroidal plasmas. Progress of Theoretical Physics Supplement, 98:83–108, 1989.

[7] Z. Yoshida. A remark on the Hamiltonian form of the magnetic鈥恔ield鈥恖ine equations. Physics of Plasmas, 1(1):208–209, 01 1994.

[8] S. Hamada. Hydromagnetic equilibria and their proper coordinates. Nuclear Fusion, 2(1-2):23, 1962.

[9] Mitsuru Kikuchi. Frontiers in Fusion Research : Physics and Fusion. Springer London, London, 1st ed. 2011 edition, 2011.

[10] M-D Hua, I T Chapman, A R Field, R J Hastie, S D Pinches, and the MAST Team. Comparison of MHD-induced rotation damping with NTV predictions on MAST. Plasma Physics and Controlled Fusion, 52(3):035009, feb 2010.

[11] M. Shimada, D.J. Campbell, V. Mukhovatov, M. Fujiwara, N. Kirneva, K. Lackner, M. Nagami, V.D. Pustovitov, N. Uckan, J. Wesley, N. Asakura, A.E. Costley, A.J.H. Donn茅, E.J. Doyle, A. Fasoli, C. Gormezano, Y. Gribov, O. Gruber, T.C. Hender, W. Houlberg, S. Ide, Y. Kamada, A. Leonard, B. Lipschultz, A. Loarte, K. Miyamoto, V. Mukhovatov, T.H. Osborne, A. Polevoi, and A.C.C. Sips. Chapter 1: Overview and summary. Nuclear Fusion, 47(6):S1, jun 2007.

[12] L.L. Lao, H. St. John, R.D. Stambaugh, A.G. Kellman, and W. Pfeiffer. Reconstruction of current profile parameters and plasma shapes in tokamaks. Nuclear Fusion, 25(11):1611, nov 1985.

[13] L.L. Lao, J.R. Ferron, R.J. Groebner, W. Howl, H. St. John, E.J. Strait, and T.S. Taylor. Equilibrium analysis of current profiles in tokamaks. Nuclear Fusion, 30(6):1035, jun 1990.

[14] H. L眉tjens, A. Bondeson, and O. Sauter. The chease code for toroidal mhd equilibria. Computer Physics Communications, 97(3):219–260, 1996.

[15] J.R. Ferron, M.L. Walker, L.L. Lao, H.E. St. John, D.A. Humphreys, and J.A. Leuer. Real time equilibrium reconstruction for tokamak discharge control. Nuclear Fusion, 38(7):1055, jul 1998.

[16] L. L. Lao, H. E. St. John, Q. Peng, J. R. Ferron, E. J. Strait, T. S. Taylor, W. H. Meyer, C. Zhang, and K. I. You. Mhd equilibrium reconstruction in the diii-d tokamak. Fusion Science and Technology, 48(2):968–977, 2005.

[17] Jacques Blum, Cédric Boulbe, and Blaise Faugeras. REAL-TIME EQUILIBRIUM RECONSTRUCTION IN A TOKAMAK. In F.P. Orsitto, G. Gorini, E. Sindoni, and M. Tardocchi, editors, Burning Plasma Diagnostics: An International Conference, volume 988, pages p 420–429, Varenna, Italy, September 2007. American institute of physics.

[18] O. Katsuro-Hopkins, S.A. Sabbagh, J.M. Bialek, H.K. Park, J.G. Bak, J. Chung, S.H. Hahn, J.Y. Kim, M. Kwon, S.G. Lee, S.W. Yoon, K.-I. You, A.H. Glasser, and L.L. Lao. Equilibrium and global mhd stability study of kstar high beta plasmas under passive and active mode control. Nuclear Fusion, 50(2):025019, jan 2010.

[19] J. Blum, C. Boulbe, and B. Faugeras. Reconstruction of the equilibrium of the plasma in a tokamak and identification of the current density profile in real time. Journal of Computational Physics, 231(3):960–980, 2012. Special Issue: Computational Plasma Physics.

[20] G Q Li, Q L Ren, J P Qian, L L Lao, S Y Ding, Y J Chen, Z X Liu, B Lu, and Q Zang. Kinetic equilibrium reconstruction on east tokamak. Plasma Physics and Controlled Fusion, 55(12):125008, nov 2013.

[21] Blaise Faugeras, Francesco Orsitto, and JET Contributors. Equilibrium reconstruction at jet using stokes model for polarimetry. Nuclear Fusion, 58(10):106032, aug 2018.

[22] Z.A. Xing, D. Eldon, A.O. Nelson, M.A. Roelofs, W.J. Eggert, O. Izacard, A.S. Glasser, N.C. Logan, O. Meneghini, S.P. Smith, R. Nazikian, and E. Kolemen. Cake: Consistent automatic kinetic equilibrium reconstruction. Fusion Engineering and Design, 163:112163, 2021.

[23] Linjin Zheng, M. T. Kotschenreuther, F. L. Waelbroeck, and Y. Todo. ATEQ: Adaptive toroidal equilibrium code. Physics of Plasmas, 29(7):072503, 07 2022.

[24] C. Hansen, I.G. Stewart, D. Burgess, M. Pharr, S. Guizzo, F. Logak, A.O. Nelson, and C. Paz-Soldan. Tokamaker: An open-source time-dependent grad-shafranov tool for the design and modeling of axisymmetric fusion devices. Computer Physics Communications, 298:109111, 2024.

[25] Yao Huang, Bing-Jia Xiao, and Zheng-Ping Luo. Fast parallel grad-shafranov solver for real-time equilibrium reconstruction in east tokamak using graphic processing unit. Chinese Physics B, 26(8):085204, 2017.

[26] R. Ma, F. Xia, F. Ling, and J. Li. Acceleration optimization of real-time equilibrium reconstruction for hl-2a tokamak discharge control. Plasma Science and Technology, 20(2):025601, jan 2018.

[27] Semin Joung, Jaewook Kim, Sehyun Kwak, J.G. Bak, S.G. Lee, H.S. Han, H.S. Kim, Geunho Lee, Daeho Kwon, and Y.-C. Ghim. Deep neural network grad鈥 撴hafranov solver constrained with measured magnetic signals. Nuclear Fusion, 60(1):016034, dec 2019.

[28] L L Lao, S Kruger, C Akcay, P Balaprakash, T A Bechtel, E Howell, J Koo, J Leddy, M Leinhauser, Y Q Liu, S Madireddy, J McClenaghan, D Orozco, A Pankin, D Schissel, S Smith, X Sun, and S Williams. Application of machine learning and artificial intelligence to extend efit equilibrium reconstruction. Plasma Physics and Controlled Fusion, 64(7):074001, jun 2022.

[29] D. A. Kaltsas and G. N. Throumoulopoulos. Neural network tokamak equilibria with incompressible flows. Physics of Plasmas, 29(2):022506, 02 2022.

[30] A Pavone, A Merlo, S Kwak, and J Svensson. Machine learning and bayesian inference in nuclear fusion research: an overview. Plasma Physics and Controlled Fusion, 65(5):053001, apr 2023.